International Journal of Minerals, Metallurgy and Materials
Volume 18, Number 3, June 2011, Page 277
DOI: 10.1007/s12613-011-0434-9

Basic properties of steel plant dust and technological properties of direct reduction

Xue-feng She[1)], *Jing-song Wang*[1)], *Qing-guo Xue*[1)], *Yin-gui Ding*[1)], *Sheng-sheng Zhang*[2)], *Jie-ji Dong*[2)], *and Hui Zeng*[2)]

1) School of Metallurgical and Ecological Engineering, University of Science and Technology Beijing, Beijing 100083, China
2) Shandong Laiwu Iron and Steel Co. Ltd., Laiwu 271104, China
(Received: 24 May 2010; revised: 26 June 2010; accepted: 2 July 2010)

Abstract: Basic physicochemical properties of the dust from Laiwu Iron and Steel Co. Ltd. were studied. It is found that C, Zn, K, Na, *etc.* exist in the fabric filter dust, off gas (OG) sludge, fine ash in converter, and electrical field dust in sinter. Among these, OG sludge gives the finest particle, more than 90% of which is less than 2.51 μm. The dust can lead to a serious negative influence on the production of sintering and blast furnaces (BF) if it is recycled in sintering. The briquette and reduction experimental results showed that the qualified strength could be obtained in the case of 8wt% molasses or 4wt% QT-10 added as binders. Also, more than 75% of metallization ratio, more than 95% of dezincing ratio, as well as more than 80% of K and Na removal rates were achieved for the briquettes kept at 1250℃ for 15 min during the direct reduction process. SEM observation indicated that the rates of indirect reduction and carbonization became dominating when the briquettes were kept at 1250℃ for 6 min.

Keywords: steel metallurgy; dust; zinc; direct reduction process; briquettes

1. Introduction

Laiwu Iron and Steel Co. Ltd. (LISC Co. Ltd.) has an annual capacity of 13 million tons of crude steel, together with more than 1 million tons of dust. Some parts of the dust have relatively high contents of elements such as C, Zn, K and Na, and the dust is called zinc-containing metallurgical dust. Presently, such kind of dust has been recycled in a sintering plant. However, the output and quality of sintering are obviously deteriorated due to the fine particle size and high zinc content which result in the low gas-permeability of the sintering process. Furthermore, the operation of a blast furnace (BF) is influenced consequently because of the serious circulation and enrichment of zinc [1-2]. Additionally, it will damage the ecological environment if the dust is deposited in the open directly. Therefore, it is of great importance to study the method of handling and recycling this kind of dust.

Since 2000, 5 rotary hearth furnaces (RHF) have been set up and put into operation at Kimitsu, Hikari, and Hirohata in Japan. The relevant data suggest that RHF is a reliable and economic method for the steel industry to handle such kind of zinc-containing metallurgical dust [3-5]. Consequently, the method of treating zinc-containing metallurgical dust with direct reduction in RHF gets more and more attention. Based on this, a meaningful cooperation has been carried out between LISC Co. Ltd. and University of Science and Technology Beijing to construct a metallic briquette production line with an annual capacity of 2×10^5 t, during which zinc-containing metallurgical dust is used as a raw material. In this paper, basic physicochemical properties of the dust from LISC Co. Ltd., the briquette production process and simulated direct reduction of RHF were studied.

The dust production of LISC Co. Ltd. in 2006 is illustrated in Table 1. The fabric filter dust, off gas (OG) sludge, fine ash in converter, and the electrical field dust in the sinter are zinc-containing metallurgical dust, the production

Corresponding author: Xue-feng She E-mail: shexuefeng@126.com

of which was 3.41×10^5 t amounting to about 33.76% of the total dust.

Generally, particles of the zinc-containing metallurgical dust are very fine. Taking OG sludge as an example, more than 90% of the particles are less than 2.51 μm. For such fine dust, its direct reuse in the sinter plant will result in inhomogeneous mixing and composition segregation, deteriorate the product quality and damage the equipment. Furthermore, it can deteriorate the air permeability and reduce the rate of vertical sintering, which leads to the decline of production.

Table 1. Dust production of LISC Co. Ltd. in 2006 10^3 t

Process	Dust species	Output	Total output
Sintering	Electrical field dust	43	472
	Surrounding dust	429	
Ironmaking	Gravity precipitator dust	86	305
	Fabric filter dust	148	
	Surrounding dust	71	
Steelmaking	OG sludge	69	188.4
	Coarse ash in converter	27	
	Fine ash in converter	84	
	Surrounding dust	8.4	
Coking	Dry quenching dust	21	45
	Wet quenching dust	24	

Additionally, zinc and alkali metals contained in the dust also have a serious negative influence on the movements of BF. The Zn, K and Na vapors reduced by carbon in the lower region of BF will be oxidized and then condense in the upper region. As a result, the permeability becomes worse; the furnace accretion and hang-ups or slip [6] are promoted. In addition, zinc and alkali metals have serious corrosion ability and the deposited liquid zinc will lead to carbon brick embrittlement at the hearth [7-9].

2. Experimental

2.1. Method

Chemical compositions of the metallurgical dust and given reduction time briquettes were obtained by chemical analysis. Mineralogical morphology inspections of the metallurgical dust were obtained by metallographic microscopy (RMEX large scale polarizing microscope). Meanwhile, X-ray diffraction (XRD) and scanning electron microscopy (SEM) were applied to analyze the phase composition and the distribution of elements such as Zn and K.

Briquettes were prepared with a binder of molasses (liquid) and QT-10 (a type of solid binder), respectively. By adjusting the dust content of the bag house filter, the ratio of carbon to oxygen was controlled at 1:1, and the moisture content was controlled at 12wt%-13wt%. After the dust was mixed uniformly, the pillow-shaped briquettes of 20 mm×30 mm×40 mm ($L\times W\times H$) in size and about 28 g in weight were produced by a twin-roller machine. And then the briquettes were dried adequately at 105°C.

Fig. 1 schematically shows the experimental apparatus. The reduction experiment was carried out by simulating the direct reduction of RHF to handle the steel plant dust. The pellet was kept at 105°C for 2 h in a drying box, and then put in a cradle made of Fe-Cr-Mo wires. The cradle was kept at 1000°C in a Si-Mo furnace for 4 min, which was recorded as the zero point for reduction. Subsequently, cradles were kept at 1250°C for 3, 6, and 9 to 24 min, respectively. The flow rate of protection gas (N_2) was set at 5.0 L/min.

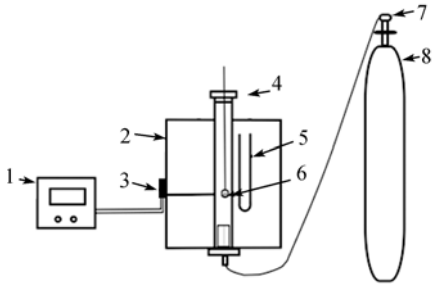

Fig. 1. Schematic diagram of the experimental apparatus. 1—temperature controller; 2—furnace; 3—thermocouple; 4—furnace cover; 5—silicon molybdenum rods; 6—sample and cradle; 7—flowmeter; 8—N_2.

2.2. Parametric description

Once the reduction reaction reached the given time, briquettes were taken out in inert gases to prevent from reoxidation. Then the metallization rate and removal percentages of elements Zn, Pb, K and Na were obtained by chemical analysis. The metallization rate (η_{Fe}) is defined as

$$\eta_{Fe} = M_{Fe}/T_{Fe}\times100\% \quad (1)$$

where M_{Fe} and T_{Fe} represent the metallic iron and the total iron contents after reduction, respectively. The removal percentages of Zn, Pb, K and Na from briquettes ($\eta_{Zn,Pb,K,Na}$) are described as

$$\eta_{Zn,Pb,K,Na} = \left[M_{(Zn,Pb,K,Na),0} - M_{(Zn,Pb,K,Na)}\right]/M_{(Zn,Pb,K,Na),0}\times100\% \quad (2)$$

where $M_{(Zn,Pb,K,Na),0}$ and $M_{(Zn,Pb,K,Na)}$ refer to the total mass of each element in initial briquettes and reduced briquettes, respectively.

3. Basic physicochemical characteristics of dust

3.1. Chemical and physical parameters

Table 2 shows the typical chemical compositions of four dusts. As can be seen, there is a relatively high amount of C and Zn in the fabric filter dust (34wt% and 16.6wt%, respectively), 15.88wt% K in the dust of the third electric field in sinter, 1.67wt% and 1.08wt% Na in the fine ash in converter and the dust of the third electric field in sinter, respectively.

Table 3 shows the bulk density, particle size distribution, and specific surface area of the four dusts [10] discussed above, from which it can be indicated that there is a large difference between different kinds of dusts. The OG sludge and fine ash in converter have the smallest particle size. Especially for OG sludge, more than 90% of its particles are less than 2.508 μm with the corresponding specific surface area of about 6.521 m^2/cm^3. The fabric filter dust and the third electric field dust in sinter have a relatively large particle size, with the specific surface of 0.730 and 1.191 m^2/cm^3, respectively. The dust in OG sludge has the largest bulk density which is 1.442 t/m^3.

3.2. Microstructural and mineralogical properties of dust

(1) Fabric filter dust

Fig. 2 shows the phase photograph of fabric filter dust. As can be seen, it mainly consists of coke and sintering ore breeze, which have interwoven distribution. There is also a little hematite, and a relatively large amount of magnetite, Silicoferrite of calcium and alumina (SFCA) and glass phase. The XRD result (Fig. 3) suggests that Zn mainly exists in the zinc ferrite phase while Fe mainly exists in hematite and magnetite phases. Fig. 4 shows the element distribution of Fe and Zn at random area. Fig. 4(a) is the original image and Fig. 4(c) is the greyscale image. Fe element mainly distributes in the bright white area of Fig. 4(b). Figs. 4(b) and 4(d) show that Zn element distributes uniformly and intersects with the concentration areas of Fe. The distribution characteristics of zinc ferrite provide good dynamic condition for dezincing.

Table 2. Chemical compositions of different dusts **wt%**

Dust category	T_{Fe}	M_{Fe}	FeO	SiO_2	CaO	MgO	Al_2O_3	K	Na	C	Zn
Fabric filter dust	17.03	1.65	7.88	2.87	2.18	0.7	2.49	0.76	0.28	34.00	16.60
Fine ash in converter	52.30	2.48	15.59	2.37	6.52	1.05	0.79	1.01	1.67	1.52	0.03
OG sludge	58.19	6.43	59.58	1.98	10.28	3.47	1.83	0.19	0.21	1.65	0.25
Dust of the third electric field in sinter	33.45	—	—	4.35	7.27	1.58	1.62	15.88	1.08	—	—

Table 3. Bulk density, particle size distribution, and specific surface area

Dust of category	Bulk density / ($t \cdot m^{-3}$)	X_{10} / μm	X_{50} / μm	X_{90} / μm	Specific surface area / ($m^2 \cdot cm^{-3}$)
Fabric filter dust	0.800	3.940	17.041	58.550	0.730
Fine ash in converter	0.778	1.219	2.822	6.538	3.031
OG sludge	1.442	0.631	1.207	2.508	6.521
Dust of third electric field in sinter	0.694	2.618	8.367	26.391	1.191

Fig. 2. Micrograph of fabric filter dust. C—coke breeze; K—sintering ore breeze; F—SFCA; M—magnetite.

(2) Fine ash in converter

Fig. 5 shows the phase photograph of fine ash in converter. As can be seen, it mainly consists of iron oxides such as hematite, magnetite, wustite and some spherical metallic iron particles. There is also a little silicate slag including dicalcium silicate, tricalcium silicate, glass phase and silica crystals, and a little periclase, coke fragment and SCFA. The result of XRD, as shown in Fig. 6, suggests that the main phases containing Fe are magnetite, hematite, and metallic iron.

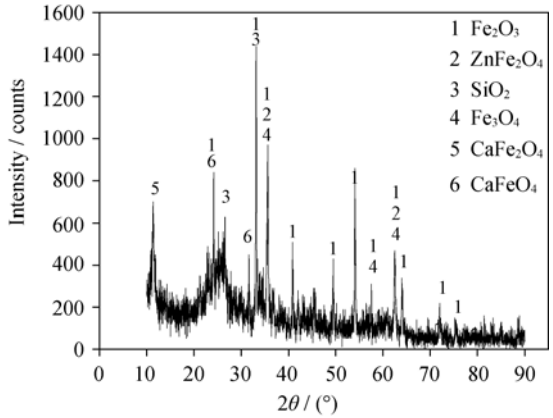

Fig. 3. XRD pattern of fabric filter dust.

(3) Fine OG sludge

Fig. 7 shows the phase photograph of OG sludge. As can be seen, it mainly consists of wustite, spherical metallic iron particles, and little coke fragments. There is also a little silicate slag of glass phase, quartz, dicalcium silicate, tricalcium silicate, dissociative calcium oxide, periclase and coke fragment. The result of XRD analysis shown in Fig. 8 indicates that Fe of OG sludge mainly exists in magnetite, wustite, and metallic iron.

(4) Dust of the third electric field in sinter

The analysis result for the dust of the third electric field

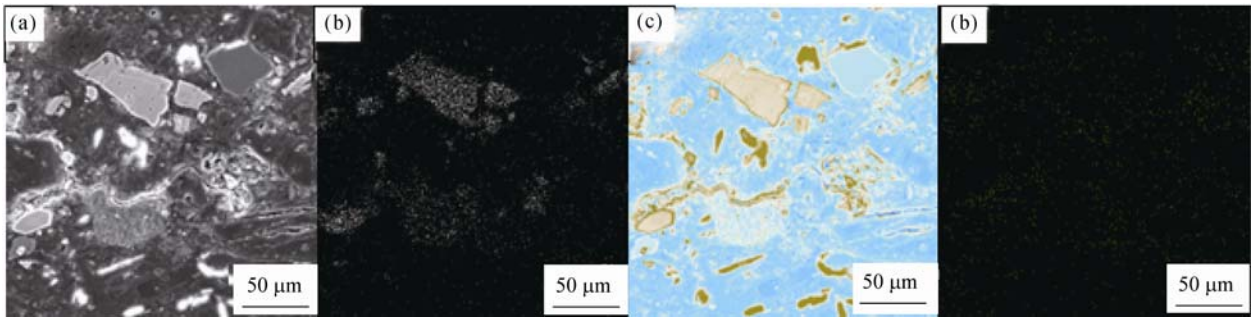

Fig. 4. SEM micrographs of the fabric filter dust: (a) original grey image; (b) Fe distribution; (c) grey image; (d) Zn distribution.

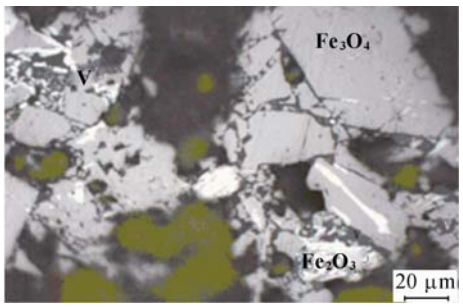

Fig. 5. Micrograph of fine ash in converter. V—glass phase; Fe_3O_4—magnetite; Fe_2O_3—hematite.

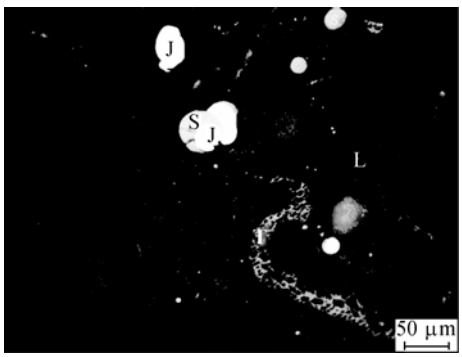

Fig. 7. Micrograph of OG sludge. J—metallic iron; S—wustite; T—coke breeze; L—dicalcium silicate.

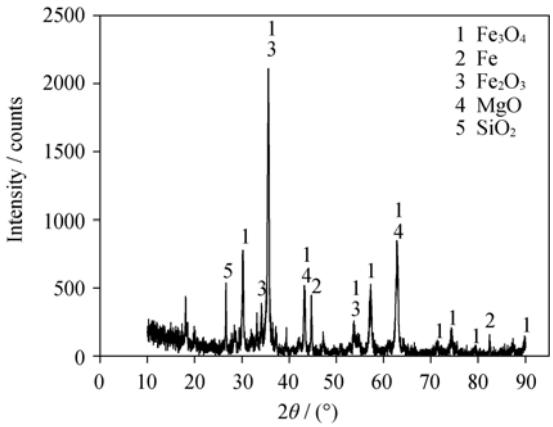

Fig. 6. XRD pattern of fine ash in converter.

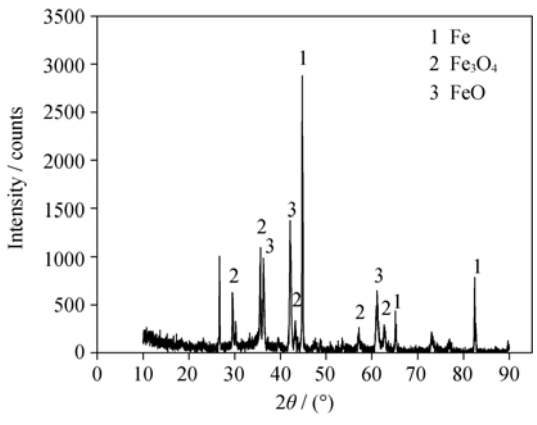

Fig. 8. XRD pattern of OG sludge.

in sinter by XRD shown in Fig. 9 suggests that it mainly consists of hematite, potassium chloride, and sodium chloride. In addition, a little of trileadtetroxide can also be found in the dust. As can be seen from the results analyzed by SEM in Figs. 10 and 11, KCl crystal is observed which can be proved by energy spectrum.

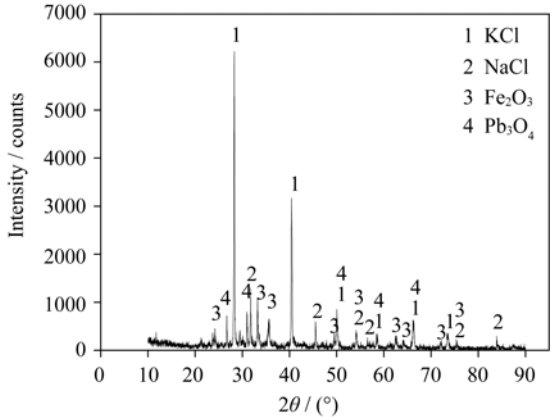

Fig. 9. XRD pattern of the third electric field in sinter.

4. Reduction experiment of dust

4.1. Briquette experiment

Experimental data using molasses as binders are shown in Fig.12. The results indicate that with the increasing ratio of molasses, all of the four parameters, *i.e.*, moist briquette falling times, drying briquette times, moist briquette compressive strength, and drying briquette compressive strength, tend to increase. In the case of 8wt% molasses, the results are: when the wet-pellet falling times from 0.5 m high are more than 8.9, the average moist briquette compressive strength is 80 N; when the dry-pellet falling times from 2 m high are more than 6.4, the average drying briquette compressive strength is 730 N.

Fig. 13 indicates a similar tendency, and the four parameters also tend to increase with the increasing content of QT-10 binder. When the amount of added QT-10 is controlled at 4wt%, the corresponding results obtained are:

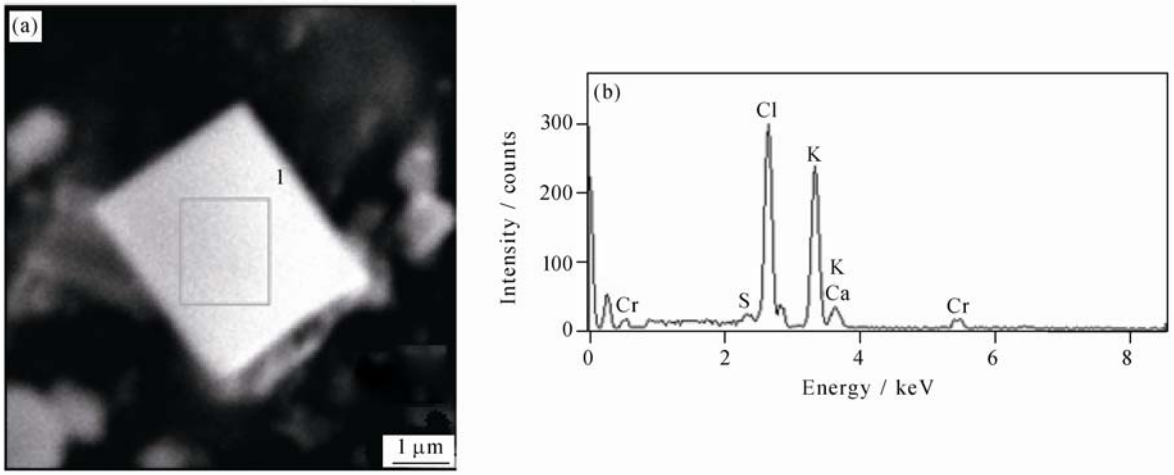

Fig. 10. SEM/EDX analysis on the third electrical dust in sinter: (a) SEM image; (b) energy spectrum in zone 1.

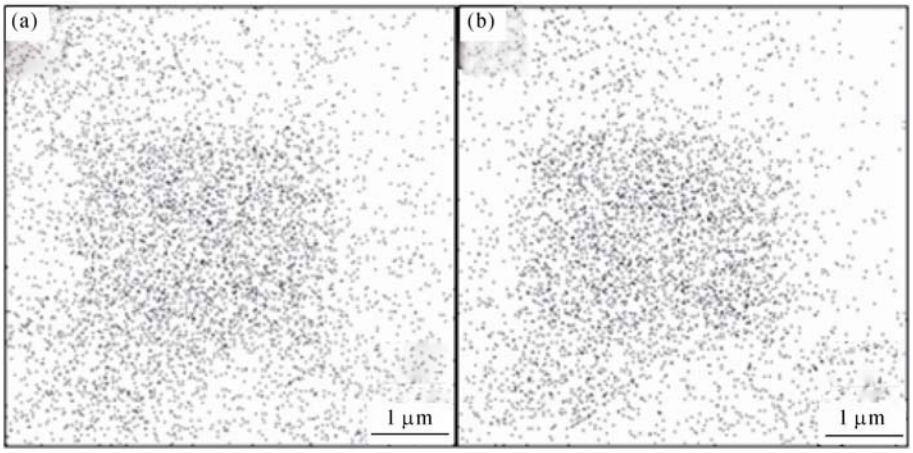

Fig. 11. Element distribution of the third electrical dust in sinter: (a) Cl; (b) K.

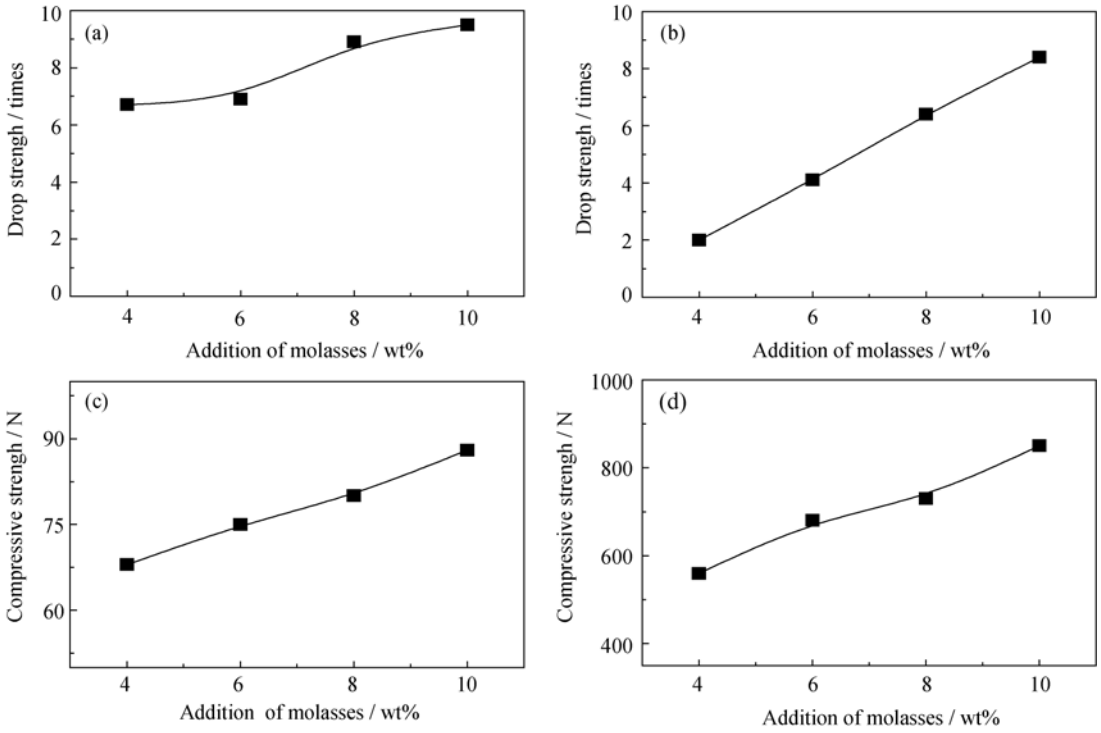

Fig. 12. Experimental results with the binder of molasses: (a) moist briquette falling times; (b) drying briquette falling times; (c) moist briquette compressive strength; (d) drying briquette compressive strength.

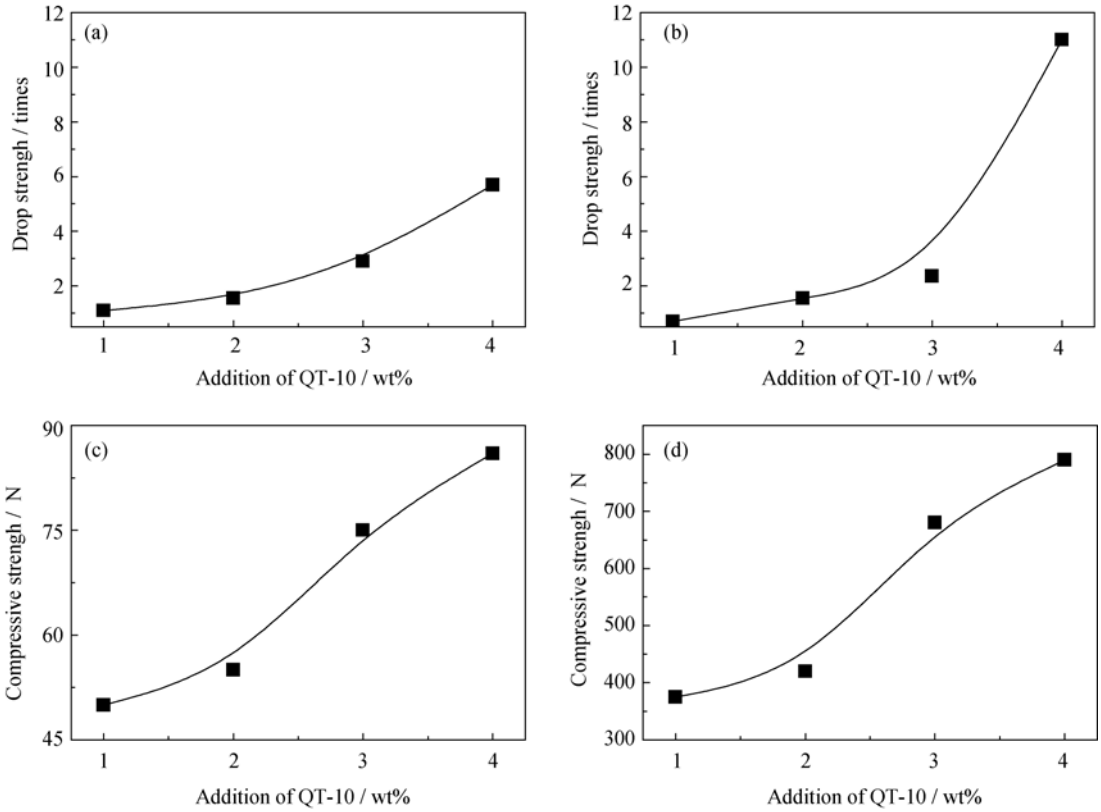

Fig. 13. Experimental results with the binder of QT-10: (a) moist briquette falling times; (b) drying briquette times; (c) moist briquette compressive strength; (d) drying briquette compressive strength.

when the wet-pellet falling times from 0.5 m high are more than 5.7, the average moist briquette compressive strength is 86 N; when the dry-pellet falling times from 2 m high are more than 11, the average drying briquette compressive strength is 790 N. It can be seen from the above results and analyses that the briquettes can satisfy the green-ball requirements of the rotary hearth furnace with a binder of 8wt% molasses or 4wt% QT-10.

4.2. Reduction experiment

Fig. 14 shows that at 1250°C, reduction of iron oxides proceeds very fast by the end of 6 min; at just 6 min, the metallization rate reaches 37.87wt%, and at the final 24 min it reaches 81.09wt%. For relatively low stability metal oxides, the indirect reduction reaction predominates, while for stable metal oxides the direct reduction reaction prevails. Reduction of metal oxides by solid carbonaceous reducing agents involves the reduction both by solid carbon and by carbon monoxide. And then the produced CO_2 by the indirect reduction reversely reacts with C to produce CO ($Fe_xO_y + yCO = xFe + yCO_2$, $CO_2 + C = 2CO$). Thus, the indirect reduction is further promoted. As a result, the overall reduction can be written as $Fe_xO_y + yC = xFe + yCO$. It is an apparent direct reduction. As time goes on, the increase of metallization rate slightly slows down.

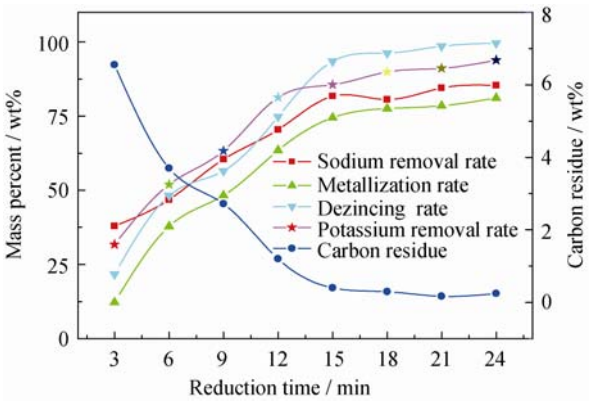

Fig. 14. Experimental results for different reduction time at 1250°C.

As can be seen from Fig. 14, more than 75wt% of metallization rate, more than 95wt% of dezincing rate, and more than 80wt% of K and Na removal rates are achieved for the briquettes kept at 1250°C for 15 min during the direct reduction process.

4.3. Observation and analysis of briquettes

Morphological changes of briquettes at 1250°C are given in Fig. 15. In the reduction progress, the pellet shrinks because of the release of CO and CO_2 gases and fusing of melt iron. After the experiment, the pellet becomes close-grained axiolitic since the reduced iron is melted down because of the decrease in its melting point caused by carburization [11-12]. During the reduction process, many cracks generate owing to the escape of CO and CO_2 gases. At the end stage, the melt iron and slag make the majority of cracks vanish.

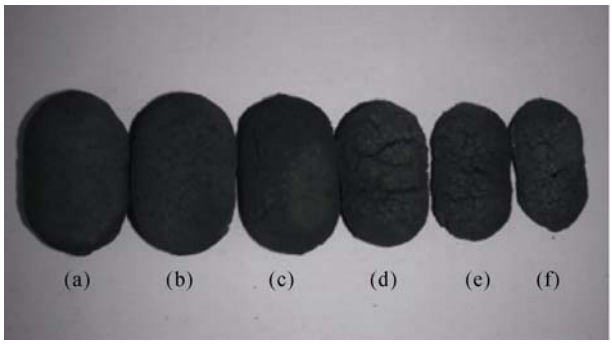

Fig. 15. Observation of briquettes at different reduction stages at 1250°C: (a) t=3 min, η_{Fe}=12.25%; (b) t=6 min, η_{Fe}=37.87%; (c) t=9 min, η_{Fe}=48.28%; (d) t=12 min, η_{Fe}=63.44%; (e) t=15 min, η_{Fe}=74.46%; (f) t=18 min, η_{Fe}=77.58%.

Fig. 16 shows the morphological changes of the pellet by SEM. Before reduction, carbon particles are 20-50 μm and can be distinguished by the particle size. Fe_2O_3 and Fe_3O_4 particles are also very fine, and most of them have a diameter of several micrometers. In the reduction process, carbon particles become smaller and the carbon surface is covered by reduction products, which break the direct contact between iron oxides and carbon particles. Therefore, the direct reduction reaction will be difficult after the reduction proceeds for a certain time [13-14]. Then indirect reduction and carbonization reaction will dominate. At these stages, the occurrence of indirect reduction is supported by the SEM observation of 6 min.

After 6 min, the carbon particles can not be distinguished by the microphotograph because carbon is consumed by reduction. Also, there are a lot of micropores in the produced iron as shown in the pictures after 6 min, which indicate that the reduced iron is in the shape of a sponge.

5. Conclusions

(1) 33.76wt% of the total dust from LG belongs to zinc-containing metallurgical dust, which is difficult to reuse in the sinter. The dust contains C, Zn, Pb, K and Na. Direct reduction of the RHF process tends to be a useful way to handle this kind of dust since it can effectively avoid the possible damage caused by the reuse of this dust in the sinter and BF.

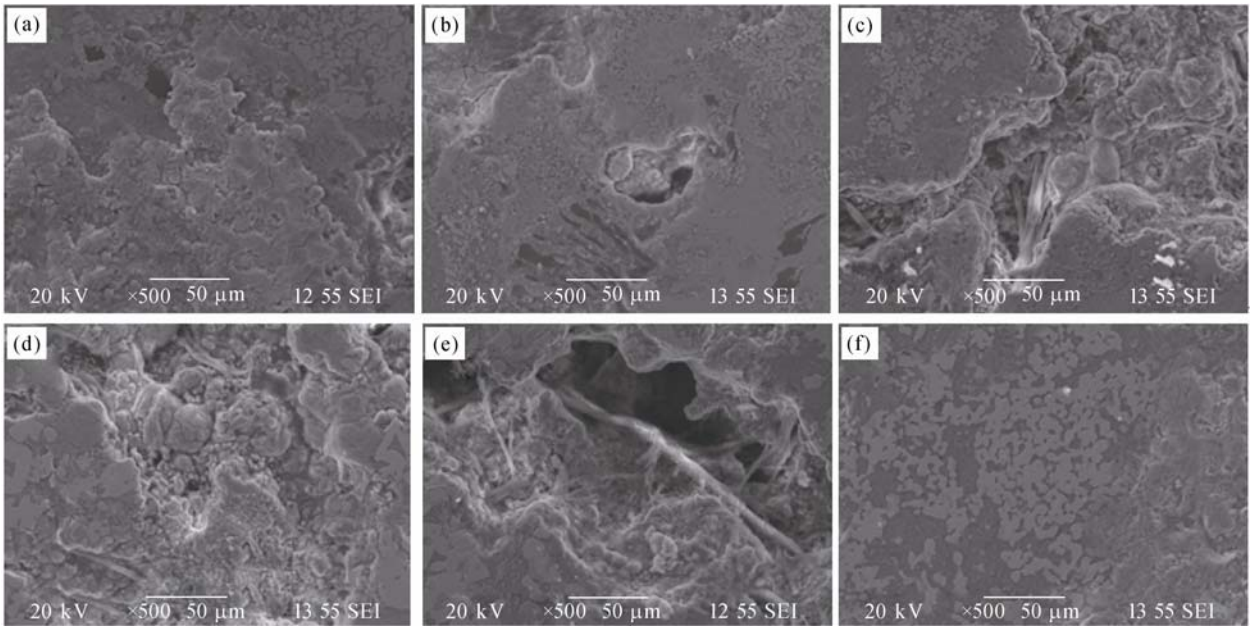

Fig. 16. SEM morphologies of briquettes at different reduction stages at 1250°C: (a) t=3 min, η_{Fe}=12.25%; (b) t=6 min, η_{Fe}=37.87%; (c) t=9 min, η_{Fe}=48.28%; (d) t=12 min, η_{Fe}=63.44%; (e) t=15 min, η_{Fe}=74.46%; (f) t=18 min, η_{Fe}=77.58%

(2) In fabric filter dust Zn mainly exists in the phase of zinc ferrite and Fe exists in the form of hematite and magnetite; iron phases of fine ash in converter are magnetite, hematite and metallic iron; iron phases of OG sludge are wustite and metallic iron with spherical particles; dust of the third electrical field in sinter consists of ferric oxide, potassium chloride, sodium chloride and complex oxides of Ca and Fe.

(3) With a binder of 8wt% molasses or 4wt% QT-10, the briquettes obtained can fully satisfy the production requirements of a rotary hearth furnace. More than 75% of metallization ratio, more than 95% of dezincing ratio, and more than 80% of K and Na removal rates are obtained for the reduced briquettes under the condition of C:O=1.0 at 1250°C for 15 min.

(4) The carbon particles are covered with reduction products after a certain time. Indirect reduction and carbonization reaction will become dominant at the stages after reduction for 6 min.

References

[1] X.W. Zhang, H.Q. Liao, X.J. Bao, *et al*., Collective processing on dust removal ash and resource utilization, *Metall. Environ. Eng.*, 40(2007), No.5, p.32.

[2] Y.X. Chen, On the centralized treatment and comprehensive of metallurgical dust, *Sintering Pelletizing*, 30(2005), No.5, p.42.

[3] B. Das, S. Prakash, P.S.R. Reddy, and V.N. Misra, An overview of utilization of slag and sludge from steel industries, *Resour. Conserv. Recycl.*, 50(2007), p.40.

[4] T. Harada , H. Tanaka, H. Sugitasu, *et al.*, FASTMET process verification for steel mill waste recycling, *KOBELCO Technol. Rev.*, 24(2001), p.26.

[5] T. Furukawa and M. Tokuda, Development of zero waste production system in Japan, [in] *The 2nd International Congress on the Science and Technology of Ironmaking*, Toronto, 1998, p.1163.

[6] R.H. Shen, G.Q. Zhang, M.D. Amico, *et al*., characterization of manganese furnace dust and zinc balance in production of manganese alloys, *ISIJ Int.*, 45(2005), No.9, p.1248.

[7] S. Jiang, Damages of detrimental elements to blast furnaces of PZH steel, *Iron Steel*, 44(2009), No.4, p.96.

[8] Y.P. Shchukin, V.I. Sedinkin, M.E. Polushkin, *et al.*, Removal of blast-furnace sludges with high zinc content from recycling, *Steel Transl.*, 29(1999), No.11, p.6.

[9] L. Bai, J.L. Zhang, H. Guo, *et al*., Circulation and enrichment of alkali metal in blast furnace, *J. Iron Steel Res.*, 20(2008), No.9, p.5.

[10] X.F. She, Q.G. Xue, J.J. Dong, *et al*., Study on basic properties of typical industrial dust from iron and steel plant and analysis of its utilization, *Chin. J. Process Eng.*, 9(2009), Suppl. 1, p.7.

[11] J.Y. Zhang, *Physical Chemistry of Metallurgy*, Metallurgical Industry Press, Beijing, 2004, p.208.

[12] C.A. Pickles, Thermodynamic analysis of the selective carbothermic reduction of electric arc furnace dust, *J. Hazard. Mater*., 150(2008), p.265.

[13] J. Yang, T. Mori, and M. Kuwabara, Mechanism of carbothermic reduction of hematite in hematite-carbon composite pellets, *ISIJ Int.*, 47(2007), No.10, p.1394.

[14] R.H. Shen, G.Q. Zhang, M. Dell'amico, *et al.*, Reduction of zinc oxide in manganese furnace dust with tar, *ISIJ Int.*, 46(2006), No.1, p.8.